T H E U N I V E R S I T Y O F M I C H I G A N

COLLEGE OF ENGINEERING
Department of Aerospace Engineering

Technical Report

FRACTURE INITIATION IN ELASTIC BRITTLE MATERIALS HAVING NON-LINEAR FRACTURE ENVELOPES

Nicholas J. Altiero
David L. Sikarskie

DRDA Project 011909

supported by:

NATIONAL SCIENCE FOUNDATION
GRANT NO. GK-37289
WASHINGTON, D.C.

administered through:

DIVISION OF RESEARCH DEVELOPMENT AND ADMINISTRATION ANN ARBOR

January 1974

ABSTRACT

A theory is outlined for determining the initation of fracture and initial fracture propagation in elastic brittle materials having non-linear Mohr fracture envelopes. This theory is applied to a specific boundary value problem, i.e. a truncated quarter plane with arbitrary traction distribution on the truncated boundary and varying confining pressure. This problem simulates the chipping phase of the penetration of a wedge shaped tool into an elastic brittle material. Numerical results are obtained for two rock materials, Blair dolomite and quartzite.

Results indicate that for increasing confining pressure, a limit condition is reached for both fracture initiation location and force. This limit location is closer to the boundary than the fracture initiation points at lower confining pressures, indicating smaller chips. It is also found that initial fracture propagation is less clearly defined at higher confining pressures. Both of these results have been observed experimentally.

NOMENCLATURE

C_A	asymptotic value of Mohr envelope
$C(\bar{\sigma}_m)$	$\bar{\tau}$ - intercept of a linear envelope tangent to the Mohr envelope at the point where the mean stress is $\bar{\sigma}_m$
$K(\bar{\sigma}_1^T, \bar{\sigma}_2^T; \mu(\bar{\sigma}_m), C(\bar{\sigma}_m))$	fracture function
K_{min}	defines point of fracture initiation
L	length of the truncated boundary; characteristic length for the problem
m	traction "form" parameter
P	total vertical line load on the truncated quarter plane (half the wedge force)
p	scalar reference pressure
t_n, t_s	normal, shear traction on truncated face
α_i	coefficients in polynomial fit for $\bar{\tau} = \bar{\tau}(\bar{\sigma}_m)$
β_i	coefficients in polynomial fit for $\bar{\sigma} = \bar{\sigma}(\bar{\sigma}_m)$
γ_1	angle between x axis and normal to first principal plane
θ	half wedge angle
ξ	length coordinate along the slanted face
μ_f	external coefficient of friction (between wedge and material)
$\mu(\bar{\sigma}_m)$	slope of linear envelope tangent to the Mohr envelope at the point where the mean stress is $\bar{\sigma}_m$
$\bar{\sigma}_{1,2}, \sigma_{1,2}$	principal, dimensionless principal stresses ($\sigma_1 > \sigma_2$) due to wedge loading
$\bar{\sigma}_{1,2}^T$	total principal stresses ($\bar{\sigma}_1^T > \bar{\sigma}_2^T$)
$\bar{\sigma}$	normal stress on a plane

$\bar{\sigma}^H$	hydrostatic stress
$\bar{\sigma}_m = \dfrac{\bar{\sigma}_1^T + \bar{\sigma}_2^T}{2}$	mean stress
$\bar{\tau}$	shear stress on a plane
ϕ_f	external friction angle ($\mu_f = \tan \phi_f$)
$\phi(\bar{\sigma}_m)$	$\mu(\bar{\sigma}_m) = \tan \phi(\bar{\sigma}_m)$
$\psi_{1,2}$	angles between x-axis and normals to Mohr planes

CONTENTS

I. INTRODUCTION

In a previous paper [1], fracture initiation and subsequent growth were analyzed for elastic brittle materials which obeyed a linear (Coulomb-Mohr) fracture envelope. Due to the linearity of the fracture criterion it was possible to do a dimensionless parametric analysis valid for all materials having such a linear envelope. There are, however, many materials for which a linear fracture envelope is not a good representation. This non-linear as in other non-linear problems, precludes a single dimensionless solution. Here it is necessary that the specific fracture envelope be known.

In the present paper a general analysis is developed for fracture initiation in non-linear brittle materials and is applied to two such materials, Blair dolomite and quartzite. As in reference [1], the idealized boundary value problem studied is the truncated quarter-plane with a variable traction applied on the truncated face, see Figure (1). Fracture initiation in such a region represents the first stage of chip formation and is important in a number of practical situations, e.g. drilling of hard rock. Of interest, also, and included in the analysis, is the effect of hydrostatic pressure on fracture initiation. This problem is of interest in drilling in the presence of large overburden pressures.

In Section II, both a discussion of the physical significance and a quantitative description of the non-linear (Mohr) fracture envelope are presented. An iterative technique for handling non-linear fracture envelopes based on a series of linear envelopes is developed in Section III. This first requires the solution of the elastic stress field based on an integral equation procedure and is discussed in detail in [2, 1]. This technique is then applied to the two materials mentioned above and results obtained for varying hydrostatic pressure and truncation angle. These results are presented and discussed in Section IV.

II. FRACTURE CRITERION

A. Discussion of the Fracture Criterion

Mohr fracture envelopes have been used extensively in the study of the fracture of brittle materials [3]. In general, these envelopes are developed phenominologically, i.e. the Mohr's circles to which the envelope is tangent are defined by "strength failure" of cylindrical test specimens under axial load and varying confining pressure. Thus, a criterion developed in this way does not define fracture initiation in the Griffith sense. It will be shown, however, that it is not fracture initiation in the Griffith sense, but rather crack coalescence that defines the onset of fracture in the present theory.

In Figure (2) are plotted lateral, volumetric, and axial strain versus axial stress for quartzite under zero confining pressure [4]. Of particular significance in explaining the microscopic behavior is the volumetric strain curve. This is interpreted as follows. Axial stresses in the vicinity of point A are sufficient to initiate growth at a number of critically oriented Griffith cracks. It should be noted that the stress field is assumed globally uniform[1] (uniaxial) and the Griffith flaws are randomly distributed and are located, for example, at grain boundaries [6]. As the stress increases these cracks continue to grow. Such growth is indicated by a deviation from linearity of volumetric strain, i.e. dilatancy, see Figure (2). This dilatancy is an increase in porosity which is a reflection of internal damage resulting from crack growth. Further increase in stress begins to produce coalescence of these cracks. For stresses beyond point B crack coalescence is extensive throughout the region as evidenced by large increases in dilatancy. This widespread damage is preliminary to the coalescence which forms the final fracture surface resulting in strength failure of the specimen. Thus, the Griffith theory gives the stress level at which preferentially oriented cracks begin to grow while the final Mohr envelope indicates when such cracks have sufficiently coalesced to cause final strength failure. In the present boundary value problem (non-uniform global stress field) of interest is the beginning of the fracture forming the resultant chip. Thus fracture initiation in the present theory is characterized by crack coalescence as differentiated from initiation in the Griffith sense and is most closely represented by the material strength failure (Mohr fracture envelope).

---

[1] Most compression tests, in fact, produce non-uniform "global" stress states. The test specimens introduced by Brace [5] closely approximate a uniform stress state as evidenced by the uniform damage distribution in the specimen.

B. Analytical Description of Mohr Envelopes

The Mohr envelopes can be represented in the following form:

$$|\bar{\tau}| + \mu(\bar{\sigma}_m)\bar{\sigma} = C(\bar{\sigma}_m) \tag{1}$$

where $\bar{\tau}$, $\bar{\sigma}$ are the dimensional shear and normal stresses on some plane; $\mu(\bar{\sigma}_m)$, $C(\bar{\sigma}_m)$ are the slope and $\bar{\tau}$ intercept of a linear envelope tangent to the Mohr envelope at the point whose mean stress is $\bar{\sigma}_m$, see Figure (3). From Figure (3) the "material constants" $\mu(\bar{\sigma}_m)$, $C(\bar{\sigma}_m)$ are given by:

$$\begin{aligned} \mu(\bar{\sigma}_m) &= \frac{\bar{\sigma}(\bar{\sigma}_m) - \bar{\sigma}_m}{\bar{\tau}(\bar{\sigma}_m)} \\ C(\bar{\sigma}_m) &= \bar{\tau}(\bar{\sigma}_m) + \mu(\bar{\sigma}_m)\bar{\sigma}(\bar{\sigma}_m) \end{aligned} \tag{2}$$

The Mohr envelopes represent given input data and are further expressible parametrically in terms of the following polynomials:

$$\begin{aligned} \bar{\tau} &= \bar{\tau}(\bar{\sigma}_m) = \sum_{i=0}^{r} \alpha_i \bar{\sigma}_m^{\,i} \\ \bar{\sigma} &= \bar{\sigma}(\bar{\sigma}_m) = \sum_{i=0}^{r} \beta_i \bar{\sigma}_m^{\,i} \end{aligned} \tag{3}$$

The two materials considered are Blair dolomite and quartzite. The Mohr envelope data for these two rocks were obtained by Brace [5] using the special compression specimens mentioned previously which insure a fairly uniform axial stress distribution. With the envelopes given, the constants in equation (3) can be found using a least squares fit. Details of this fitting including the computer program [7] are found in Appendix A.

III. ANALYSIS

A fracture mechanics analysis involves several steps. It is first necessary to determine the stress field due to the external loadings. This stress is then compared with a fracture criterion to determine the location and stress level at which fracture initiates. The next stage is fracture growth which in the present problem would terminate in the formation of a chip [1]. The main interest in the present paper is in the initiation of fracture. However, comments regarding initial fracture propagation are also made.

The criterion which governs here is the Mohr criterion given by equation (1). If the planes which maximize the left hand side of equation (1) are found and the resulting stresses on these planes expressed in terms of principal stresses, equation (1) takes the form,

$$\frac{\mu(\bar{\sigma}_m)}{2}\left(\bar{\sigma}_1^T + \bar{\sigma}_2^T\right) + \frac{\sqrt{1+\mu^2(\bar{\sigma}_m)}}{2}\left(\bar{\sigma}_1^T - \bar{\sigma}_2^T\right) = C(\bar{\sigma}_m) \tag{4}$$

$\bar{\sigma}_1^T$, $\bar{\sigma}_2^T$ are the principal stresses with $\sigma_1^T > \sigma_2^T$, reckoned algebraically. The superscript T indicates total stress due to both loading on the truncated face, see Figure (1), and hydrostatic pressure. There are two angles for which equation (4) is valid,

$$\psi_{1,2} = \gamma_1 \pm \left(\frac{\pi}{4} - \frac{\phi(\bar{\sigma}_m)}{2}\right) ; \tan\phi(\bar{\sigma}_m) = \mu(\bar{\sigma}_m) \tag{5}$$

where γ_1 is the angle between the normal to the first principal plane and the x axis. It is important to note that the interpretation of the angles $\psi_{1,2}$

in terms of fracture direction is unclear at present. The authors do not believe, as is commonly interpreted, that these angles define the fracture directions, per se. The Mohr planes defined by these angles are shown on Figure (4), and clearly, are not consistent with known "chipping" behavior. The interpretation of reference [1], namely that these planes represent directions of critically oriented Griffith cracks, is also not totally consistent here since the Mohr criterion assumes that cracks have already coalesced However, it can be shown (but is omitted here) that these directions are close to those predicted by the Griffith theory.

If the total stress is divided into its component parts;

$$\bar{\sigma}_1^T = \bar{\sigma}_1 + \bar{\sigma}^H$$
$$\bar{\sigma}_2^T = \bar{\sigma}_2 + \bar{\sigma}^H \tag{6}$$

and substituted into equation (4), the following is obtained;

$$\frac{\mu(\bar{\sigma}_m)}{2}(\bar{\sigma}_1 + \bar{\sigma}_2) + \sqrt{\frac{1 + \mu^2(\bar{\sigma}_m)}{2}}(\bar{\sigma}_1 - \bar{\sigma}_2) = C(\bar{\sigma}_m) - \mu(\bar{\sigma}_m)\bar{\sigma}^H \tag{7}$$

Nondimensionalizing $\bar{\sigma}_1$, $\bar{\sigma}_2$ with respect to P/L (see Figure (1)), i.e. $\sigma_1 = \bar{\sigma}_1 L/P$, $\sigma_2 = \bar{\sigma}_2 L/P$, equation (7) becomes;

$$P/L\left[\frac{\mu(\bar{\sigma}_m)}{2}(\sigma_1 + \sigma_2) + \sqrt{\frac{1 + \mu^2(\bar{\sigma}_m)}{2}}(\sigma_1 - \sigma_2)\right] = C(\bar{\sigma}_m) - \mu(\bar{\sigma}_m)\bar{\sigma}^H \tag{8}$$

A "fracture function" is now defined;

$$K(\bar{\sigma}_1^T, \bar{\sigma}_2^T; \mu(\bar{\sigma}_m), C(\bar{\sigma}_m)) = \frac{P}{L} = \frac{2\left[C(\bar{\sigma}_m) - \mu(\bar{\sigma}_m)\bar{\sigma}^H\right]}{\mu(\bar{\sigma}_m)(\sigma_1 + \sigma_2) + \sqrt{1 + \mu^2(\bar{\sigma}_m)}\;(\sigma_1 - \sigma_2)} \tag{9}$$

This fracture function has the following physical interpretation. It is that value of P/L necessary to initiate fracture at a given point in the field. Clearly, the minimum value of K (K_{min}) in the field is where the actual fracture begins.

To find K the stress field σ_1, σ_2 must first be known. Following reference [1] a traction distribution (due to the "wedge" force) is assumed;

$$t_n = \begin{cases} 0 & \text{on DB} \\ p\,(\xi/L)^m\left(1 - \dfrac{\cos 2\pi\xi}{L}\right) & \text{on BA} \\ 0 & \text{on AC} \end{cases}$$

$$t_s = \begin{cases} 0 & \text{on DB} \\ \mu_f t_n = p\mu_f\,(\xi/L)^m\left(1 - \dfrac{\cos 2\pi\xi}{L}\right) & \text{on BA} \\ 0 & \text{on AC} \end{cases} \tag{10}$$

where t_n, t_s are the normal and tangential traction components, ξ a coordinate on BA defined in Figure (1) and μ_f the coefficient of friction between wedge and rock. m is a form parameter which for increasing value gives a more asymmetric and concentrated traction distribution. $m = 5$ and $\mu_f = 0$ are used throughout the analysis. These are reasonable approximations for the traction distribution due to a penetrating wedge shaped tool. p is a scalar pressure which can be related to the half wedge force P as follows;

$$p = \frac{P \cos \phi_f}{L \sin (\theta + \phi_f) \int_0^1 \eta^m (1 - \cos 2\pi\eta) d\eta} \quad (11)$$

where θ is the half wedge angle (truncation angle) and ϕ_f is the friction angle; $\tan \phi_f = \mu_f$. For p defined by equation (12) all traction distributions (any value of ϕ_f, m) add up to the same value of P/L (vertical "force" component).

The stress field (before fracture has started) represents a linear calculation and an integral equation procedure, outlined in detail in references [1,2] can be used. For brevity, this is not repeated here.

With σ_1, σ_2 known throughout the field for a given traction distribution for which P/L = 1, K_{min} can be found using the following iteration equations;

$$K^{(n)} = (P/L)^{(n)} = \frac{2\,[C^{(n-1)}(\bar{\sigma}_m^{(n-1)}) - \mu^{(n-1)}(\bar{\sigma}_m^{(n-1)})\bar{\sigma}^H]}{\mu^{(n-1)}(\bar{\sigma}_m^{(n-1)})(\sigma_1 + \sigma_2) + \sqrt{1 + (\mu^{(n-1)}(\bar{\sigma}_m^{(n-1)}))^2}\,(\sigma_1 - \sigma_2)} \quad (a)$$

$$\bar{\sigma}_m^{(n)} = (\sigma_1 + \sigma_2)(P/L)^{(n)} + \bar{\sigma}^H \quad (b)$$

$$\bar{\tau}^{(n)} = \sum_{i=0}^{r} \alpha_i (\bar{\sigma}_m^{(n)})^i \quad (c)$$

$$\bar{\sigma}^{(n)} = \sum_{i=0}^{r} \beta_i (\bar{\sigma}_m^{(n)})^i \quad (d)$$

$$\mu^{(n)} = \frac{\bar{\sigma}^{(n)} - \bar{\sigma}_m^{(n)}}{\bar{\tau}^{(n)}} \qquad \text{(e)}$$

$$C^{(n)} = \bar{\tau}^{(n)} + \mu^{(n)} \bar{\sigma}^{(n)} \qquad \text{(f)}$$

(12)

where the [illegible] n parentheses represent the iteration cycle number. Note that σ_1, σ_2, $\bar{\sigma}^H$, α_i, β_i are constants throughout the iteration. Assuming initially ($n = 1$), $\mu^{(0)} = 0$, $C^{(0)} = C_A$ (the appropriate asymptotic value of the Mohr envelope, see Figure (3))[2], $K^{(1)}$ is found directly from (12a). This value of $K^{(1)}$ determines a new mean stress $\bar{\sigma}_m^{(1)}$ from equation (12b), which in turn determines $\bar{\tau}^{(1)}$, $\bar{\sigma}^{(1)}$ from equations (12 c,d) and finally the new constants $\mu^{(1)}$, $C^{(1)}$ from equations (12 e, f). This iteration proceeds until convergence is obtained, namely

$$\frac{|K^{(n)} - K^{(n-1)}|}{|K^{(n-1)}|} < \epsilon \qquad (13)$$

where ϵ usually is selected to be 0.01.

This iteration procedure should take place at every point in the field with that point at which K is minimum being the fracture initiation point. To implement this numerically those points shown as dots on Figures (4) were the initially selected field points.[3] The iteration procedure

[2] Beginning the iteration from the asymptotic value of the Mohr envelope avoids certain numerical difficulties, i.e. too large an initial value of μ may result in an unbounded first iterant.

[3] It is necessary to have K throughout the field for later comments on fracture propagation.

was done at all of these points and the location and value of K_{min} found. The field was then subdivided in the vicinity of this point, as shown in Figure (4), and the iteration repeated for this smaller field. The new value and location of K_{min} is the one finally selected. The computer program which does both the stress field calculation and K_{min} iteration procedure is found in **Appendix B.**

IV. DISCUSSION OF NUMERICAL RESULTS

Numerical results for the two materials considered, namely, Blair dolomite and quartzite, are summarized in Table 1, and in Figures (4-6). The confining pressures considered in these results, i.e. zero to three kilobars, represent moderate pressures and the materials are still in their brittle state, see Robertson [8].

Fracture initation locations for the various cases are shown in Figure (4). As the confining pressure increases the fracture initiation point approaches a limiting point nearer the surface. This indicates a decreasing "chip" size with increasing confining pressure. Similar results have been noted experimentally by Gnirk and Cheatham [9]. The force necessary to initiate fracture also approaches a limiting value as confining pressure increases as is seen in Table 1. An important result is that fracture initiation location for a given traction distribution is solely dependent on $\mu(\overline{\sigma}_m)$ (location on the Mohr envelope).[4] The small differences in fracture

[4] This conclusion is consistent with the results of reference [1], where the dependence on μ is discussed in more detail.

initiation point for Blair dolomite and quartzite at low confining pressure is due to differences in the slope of their respective Mohr envelope at low mean stress. Differences in the two materials show up in the relative magnitude of the forces required to initiate fracture (K_{min}), see Table 1. Mohr envelope intercepts of the various fracture initation points of Figure (4) are shown in Figure (3) for Blair dolomite.

Effects of wedge angle (truncation angle) on the magnitude of the fracture initation force for Blair dolomite can also be seen in Table 1. As expected, fracture initation forces increase with increasing wedge angle. It is interesting to note that for all three wedge angles (and $\overline{\sigma}^H = -2kb$) the location of the fracture initiation point was identical (within the range of accuracy of the subdivision) relative to the truncated face. This is expected, however, since the fracture initiation point is somewhat removed from the boundaries DB and AC of Figure (1).

The analysis (determination of K throughout the field) can be used to predict initial propagation of the fracture also. In Figures (5), (6) contour ma of K for Blair dolomite at zero and three kilobars confining pressure are show Following reference [1] it is proposed that the initial propagation of the fracture follows the minimum gradient of the contour plot. An interesting result is that this proposed fracture path is well defined at zero confining pressure, Figure (5), but less so at higher confining pressure, Figure (6). This would indicate more ambiguity in chipping behavior at higher confining pressures. This has also been seen experimentally by Gnirk and Cheatham [9

APPENDIX A

POLYNOMIAL FITS FOR $\bar{\sigma} = \bar{\sigma}(\bar{\sigma}_m)$ AND $\bar{\tau} = \bar{\tau}(\bar{\sigma}_m)$

The coefficients α_i, β_i of equation (3) were obtained in the following way. Normals were drawn to the Mohr envelope of the material at a number of points spanning the range of interest. The intercepts of these normals with the $\bar{\sigma}$ axis determine the values of $\bar{\sigma}_m$ and the corresponding points on the Mohr envelope determine the corresponding values of $\bar{\sigma}$, $\bar{\tau}$. Data points obtained in this way are shown in Table A-1 for Blair dolomite and Table A-2 for quartzite. Polynomial curves were then fit to these data points using the following computer program developed in ref. [7].

A. Input Data

M - Number of data points to be fit

MIN - Lowest order polynomial fit desired

MAX - Highest order polynomial fit desired

X - $\bar{\sigma}_m$ values of data points

Y - Corresponding $\bar{\sigma}$ or $\bar{\tau}$ values of data points

B. Output Data

N - Order of polynomial fit

DET - Determinant of Matrix

S - Standard deviation

A - α_o or β_o

B(I) - α_i or β_i, i = 1, N

```
$SIGNON
$RUN *STATUS
$RUN *FTN
          IMPLICIT REAL*8(A-H, O-Z)
          INTEGER POINT
          DIMENSION X(100),Y(100),B(10),POINT(10),IMAGE(2500)
          DATA POINT/'1','2','3','4','5','6','7','8','9','0'/
          NAMELIST/DATA/M,MIN,MAX,X,Y
  1       READ (5,DATA)
          WRITE (6,DATA)
          DO 5 N=MIN,MAX
          WRITE (6,202) N
          S=REGR (M,X,Y,N,A,B)
          IF (S.NE.0.0) GO TO 3
          WRITE (6,203)
          GO TO 1
  3       WRITE (6,204) S,A,(I,B(I),I=1,N)
          DELTAX=(X(M)-X(1))/25.0
          MP1=M+1
          MP26=M+26
          DO 4 I=MP1,MP26
          STEPS=I-M-1
          X(I)=X(1)+STEPS*DELTAX
          Y(I)=A
          DO 4 J=1,N
  4       Y(I)=Y(I)+B(J)*X(I)**J
          WRITE (6,205)
          CALL PLOT1 (0, 5, 10, 6, 20)
          CALL PLOT2 (IMAGE(1), -, -, -, -)
          CALL PLOT3 (POINT(N), X(MP1), Y(MP1), 26, 8)
          CALL PLOT3 ('*', X(1), Y(1), M, 8)
          CALL PLOT4 (10, 10HORDINATE Y).
  5       WRITE (6,206)
          GO TO 1
 202  FORMAT (32H1 POLYNOMIAL REGRESSION OF ORDER/1H0, 5X, 7H N    = ,I
 203  FORMAT (69H0 MATRIX C IS NEAR-SINGULAR.    REGRESSION COEFFICIENT
     1NOT DETERMINED)
 204  FORMAT (1H0, 5X, 5H S = , F14.6/ 6X, 5H A = , D16.8//
     1 (6X, 3H B(, I2, 4H) = , D16.8))
 205  FORMAT (1H1)
 206  FORMAT (1H0, 56X, 13H ABSCISSA (X))
          END
          FUNCTION REGR (M,X,Y,N,A,B)
          IMPLICIT REAL*8(A-H, O-Z)
          REAL*8 A,B,REGR,X,Y
          DATA EPS/ 1.0E-20/
          DIMENSION C(11,11),SX(20),SYX(10),CYX(10),X(100),Y(100),B(10)
          NTWO=2*N
          NP1=N+1
          SY=0.0
          SYY=0.0
          DO 1 I=1,N
          NPI=N+I
          SX(I)=0.0
          SX(NPI)=0.0
  1       SYX(I)=0.0
          DO 3 I=1,M
          SY=SY+Y(I)
          SYY=SYY+Y(I)**2
          DUM=1.0
```

```
      DO 2 J=1,N
      DUM=DUM*X(I)
      SX(J)=SX(J)+DUM
 2    SYX(J)=SYX(J)+Y(I)*DUM
      DO 3 J=NP1, NTWO
      DUM=DUM*X(I)
 3    SX(J)=SX(J)+DUM
      FM=M
      CYY=SYY-SY*SY/FM
      DO 4 I=1,N
      CYX(I)=SYX(I)-SY*SX(I)/FM
      C(I,NP1)=CYX(I)
      DO 4 J=1,N
      IPJ=I+J
 4    C(I,J)=SX(IPJ)-SX(I)*SX(J)/FM
      DET=SIMUL (N,C,B,EPS,1,11)
      WRITE (6,200) DET
200 FORMAT (13H0          DET = , E14.8)
      IF (DET .NE. 0.0) GO TO 6
      REGR=0.0
      RETURN
 6    DUM=SY
      TEMP=CYY
      DO 7 I=1,N
      DUM=DUM-B(I)*SX(I)
 7    TEMP=TEMP-B(I)*CYX(I)
      A=DUM/FM
      DENOM=M-N-1
      S=DSQRT(TEMP/DENOM)
      REGR=S
      RETURN
      END
      FUNCTION SIMUL(N,A,X,EPS,INDIC,NRC)
      IMPLICIT REAL*8(A-H, O-Z)
      REAL*8 A,X,EPS,SIMUL
      DIMENSION IROW(50),JCOL(50),JORD(50),Y(50),A(NRC,NRC),X(N)
      MAX=N
      IF(INDIC.GE.0) MAX=N+1
      IF (N.LE.50) GO TO 5
      WRITE (6,200)
      SIMUL=0.
      RETURN
 5    DETER=1.
      DO 18 K=1,N
      KM1=K-1
      PIVOT=0.
      DO 11 I=1,N
      DO 11 J=1,N
      IF (K.EQ.1) GO TO 9
      DO 8 ISCAN=1,KM1
      DO 8 JSCAN=1,KM1
      IF (I.EQ.IROW(ISCAN)) GO TO 11
      IF (J.EQ.JCOL(JSCAN)) GO TO 11
 8    CONTINUE
 9    IF (DABS(A(I,J)).LE.DABS(PIVOT)) GO TO 11
      PIVOT=A(I,J)
      IROW(K)=I
      JCOL(K)=J
 11   CONTINUE
      IF (DABS(PIVOT).GT.EPS) GO TO 13
```

```
      SIMUL=0.
      RETURN
13    IROWK = IROW(K)
      JCOLK = JCOL(K)
      DETER = DETER*PIVOT
      DO 14 J=1,MAX
14    A(IROWK,J) = A(IROWK,J)/PIVOT
      A(IROWK,JCOLK) = 1./PIVOT
      DO 18 I=1,M
      AIJCK = A(I,JCOLK)
      IF (I.EQ.IROWK) GO TO 18
      A(I,JCOLK) = -AIJCK/PIVOT
      DO 17 J=1,MAX
17    IF (J.NE.JCOLK) A(I,J)=A(I,J)-AIJCK*A(IROWK,J)
18    CONTINUE
      DO 20 I=1,M
      IROWI=IROW(I)
      JCOLI=JCOL(I)
      JORD(IROWI)=JCOLI
20    IF (INDIC.GE.0) X(JCOLI)=A(IROWI,MAX)
      INTCH=0
      NM1=N-1
      DO 22 I=1,NM1
      IP1=I+1
      DO 22 J=IP1,M
      IF (JORD(J).GE.JORD(I)) GO TO 22
      JTEMP=JORD(J)
      JORD(J)=JORD(I)
      JORD(I)=JTEMP
      INTCH=INTCH+1
22    CONTINUE
      IF (INTCH/2*2.NE.INTCH) DETER=-DETER
24    IF (INDIC.LE.0) GO TO 26
      SIMUL=DETER
      RETURN
26    DO 28 J=1,M
      DO 27 I=1,M
      IROWI=IROW(I)
      JCOLI=JCOL(I)
27    Y(JCOLI)=A(IROWI,J)
      DO 28  I=1,M
28    A(I,J)=Y(I)
      DO 30 I=1,M
      DO 29 J=1,M
      IROWJ=IROW(J)
      JCOLJ=JCOL(J)
29    Y(IROWJ)=A(I,JCOLJ)
      DO 30 J=1,M
30    A(I,J)=Y(J)
      SIMUL=DETER
      RETURN
200   FORMAT (10HON TOO BIG)
      END
$ENDFILE
$RUN -LOAD+*SSP MAP 5=*SOURCE* 6=*SINK*
$SIGNOFF
$ENDFILE
                                                        177  LI
```

Polynomials of order 1, . . ., 9 were fit to the data of Tables A-1 and A-2 and the best of these fits were chosen in each case. The resultant coefficients are given in Table A-3.

APPENDIX B

COMPUTER PROGRAM

NONLINEAR FRACTURE ENVELOPE

A computer program was employed for the numerical computation of the stress field and "fracture function." A listing of that program is presented in this appendix.

A. Input Data

The following information must be provided as input (all values are dimensionless unless otherwise designated):

NML -	total number of subdivisions on the boundary, see ref. [1].
NDB, NBA -	the number of these subdivisions allotted to boundary segments DB and BA respectively (figure 1); see ref. [1].
(S (I), I = 1, NML) -	the lengths of the boundary subdivisions beginning with right-most on boundary DB and listing counter-clockwise, see ref. [1].
PC -	degree of accuracy desired in the iteration to determine fictitious loads, see ref. [1].
AL -	value of the convergence parameter, α, see ref. [1].
NFPI -	the number of field points at which the stress tensor components and "fracture function" are to be computed.
(XF (I), YF (I), I = 1, NFPI) -	co-ordinates of these field points with respect to the co-ordinate system designated in figure 1.
DIV -	Once the "fracture function," K, has been evaluated at each of the specified field points, the computer determines at which of these points K is a minimum. A grid is then set up about this point as in figure B-1, the computations are repeated and a new location of minimum K is

determined. A minor adjustment to the program would allow for further subdivisions and subsequently better accuracy.

THETA - the half wedge angle, θ.

MUF - coefficient of friction on loaded surface, μ_f.

M - form parameter, m.

MUI - initial choice of μ: $\mu^{(0)}$.

CI - initial choice of C: $C^{(0)}$ (in kb).

T0, . . . , T7 - coefficients α_i, equation (3).

S0, . . . , S7 - coefficients β_i, equation (3).

SIGMAX - value of $\bar{\sigma}$ at which Mohr envelope is essentially equal to asymptote (in kb).

TAUMAX - maximum value of $\bar{\tau}$ for Mohr envelope (in kb).

SGMAH - hydrostatic stress (in kb).

B. Output Data

The following information is obtained as output (again, all values are dimensionless unless otherwise designated):

(LOCT (I), XB (I), YB(I), I = 1, NML) - Given the number and lengths of the boundary subdivisions, the computer determines the coordinates of the center point of each and assigns to each a location number. This numbering begins at the right-most subdivision on the boundary segment DB and proceeds consecutively in the counter-clockwise direction (figure 1); see ref. [1] .

(PX (I), PY (I), I = 1, NML) - components of the real traction on the boundary, represented by the concentrated real load at the center of each one of the subdivisions, see ref. [1] .

(PXS (I), PYS (I), I = 1, NML) - components of the fictitious traction on the boundary, represented by the concentrated load, P^*_{xi}, P^*_{yi}, at the center of each one of the subdivisions, see ref. [1] .

(LOCT (I), XF (I), YF (I) I = 1, NFP) -	The computer also assigns a location number to each of the field points. The set of specified field points (input) are numbered from 1 to NFPI whereas the points of the grid (figure B-1) are numbered from (NFPI + 1) to NFP = (NFPI +22).
(SGMAXX (I), SGMAYY (I), SGMAXY (I), I =1, NFP) -	components of the stress tensor, σ_{xx}, σ_{yy}, σ_{xy}, at each of the field points, see ref. [1].
(SGMA1 (I), SGMA2 (I), ALPHA1 (I), ALPHA2 (I), I = 1, NFP) -	principal stresses and their directions at these same field points. SGMA1 (I) is the larger stress in an algebraic sense.
(K(I), PSI1(I), PSI2 (I), I = 1, NFP) -	the "fracture function," K (equation 12 a) and the Mohr angles (equation 5) at each field point for each iteration.
(SGMAM (I), MU (I), C (I), I = 1, NFP) -	the mean stress and slope and $\bar{\tau}$ - intercept of a linear envelope tangent to the real Mohr envelope at a point defined by the mean stress at each field point for each iteration.
KMIN -	minimum value of K; value of K at the point of fracture initiation.

The computer program follows.

```
$SIGNON
$RUN *STATUS
$RUN *FTN
C ISOTROPIC CASE - NONLINEAR CRITERION
        REAL MUF
        REAL MUI
        REAL MU(164)
        REAL K(164,10)
        REAL KMIN
        DIMENSION S(96),XB(96),YB(96),ANX(96),ANY(96),PX(96),PY(96),
     1  B1(96,96),B2(96,96),B3(96,96),PXS(96),PYS(96),PXSN(96),
     2  PYSN(96),SUMX(96),SUMY(96),XF(164),YF(164),SGMAXX(164),
     3  SGMAYY(164),SGMAXY(164),SGMAA(164),SGMAB(164),
     4  SGMA1(164),SGMA2(164),ALPHAA(164),ALPHAB(164),ALPHA1(164),
     5  ALPHA2(164),PSI1(164),PSI2(164),LOCT(164),C(164),SGMAM(164),
     6  SIG(164),TAU(164)
 100    FORMAT ('1')
 201    FORMAT ('OLOCT',19X,'XB',35X,'YB'/'0'/(I4,8X,F20.8,16X,F20.8))
 301    FORMAT ('OLOCT',19X,'PX',35X,'PY'/'0'/(I4,8X,F20.8,16X,F20.8))
 401    FORMAT ('OCICLE  =',I4/'0'/'LOCT',18X,'PXS',34X,'PYS'/'0'/
     1  (I4,8X,F20.8,16X,F20.8))
 501    FORMAT ('OLOCT',19X,'XF',35X,'YF'/'0'/(I4,8X,F20.8,16X,F20.8))
 601    FORMAT ('OLOCT',17X,'SGMAXX',30X,'SGMAYY',30X,'SGMAXY'/'0'/
     1  (I4,8X,F20.8,16X,F20.8,16X,F20.8))
 701    FORMAT ('OLOCT',17X,'SGMA1',21X,'SGMA2',20X,'ALPHA1',20X,
     1  'ALPHA2'/'0'/(I4,8X,F20.8,6X,F20.8,6X,F20.8,6X,E20.8))
 800    FORMAT ('OITERATION  =',I3)
 801    FORMAT ('OLOCT',17X,'SGMAM',22X,'MU',25X,'C'/'0'/(I4,8X,F20.8,
     1  6X,F20.8,6X,F20.8))
 802    FORMAT ('OLOCT',19X,'K',34X,'PSI1',32X,'PSI2'/'0'/
     1  (I4,8X,F20.8,16X,F20.8,16X,F20.8))
 901    FORMAT ('OCICLES =',I4,10X,'KMIN  =',F20.8)
        NAMELIST/DATA1/NBL,NDB,NBA,S,PC,AL,NFPI,XF,YF,DIV,THETA,MUF,
        NAMELIST/DATA2/ MUI,CI,T0,T1,T2,T3,T4,T5,T6,T7,S0,S1,S2,S3,
     1  S4,S5,S6,S7,SIGMAX,TAUMAX,SGMAH
        READ (5,DATA1)
        WRITE (6,DATA1)
        DO 2 I=1,164
   2    LOCT(I)=I
C
C DETERMINATION OF XB(I) AND YB(I)
        XD=0.0
        DO 3 I=1,NDB
   3    XD=XD+S(I)
        II=NDB+1
        JJ=NDB+NBA
        DO 4 I=II,JJ
   4    XD=XD+S(I)*SIN(THETA)
        XB(1)=XD-S(1)/2.0
        YB(1)=0.0
        DO 5 I=2,NDB
        XB(I)=XB(I-1)-(S(I)+S(I-1))/2.0
   5    YB(I)=0.0
        XB(NDB+1)=XB(NDB)-S(NDB)/2.0-S(NDB+1)*SIN(THETA)/2.0
        YB(NDB+1)=-S(NDB+1)*COS(THETA)/2.0
        II=NDB+2
        JJ=NDB+NBA
        DO 6 I=II,JJ
        XB(I)=XB(I-1)-(S(I)+S(I-1))*SIN(THETA)/2.0
        YB(I)=YB(I-1)-(S(I)+S(I-1))*COS(THETA)/2.0
```

```
6       CONTINUE
        II=NDB+NBA+2
        XB(II-1)=0.0
        YB(II-1)=YB(II-2)-S(II-1)/2.0-S(II-2)*COS(THETA)/2.0
        DO 7 I=II,NML
        XB(I)=0.0
        YB(I)=YB(I-1)-(S(I)+S(I-1))/2.0
7       CONTINUE
        WRITE (6,100)
        WRITE (6,201) (LOCT(I),XB(I),YB(I), I=1,NML)
C
C DETERMINATION OF ANX(I) AND ANY(I)
        DO 8 I=1,NDB
        ANX(I)=0.0
8       ANY(I)=1.0
        II=NDB+1
        JJ=NDB+NBA
        DO 9 I=II,JJ
        ANX(I)=-COS(THETA)
9       ANY(I)=SIN(THETA)
        II=NDB+NBA+1
        DO 10 I=II,NML
        ANX(I)=-1.0
10      ANY(I)=0.0
C
C DETERMINATION OF PX(I) AND PY(I)
C       N CANNOT EXCEED 5
        PI=3.1415927
        DO 11 I=1,NDB
        PX(I)=0.0
11      PY(I)=0.0
        II=NDB+NBA+1
        DO 12 I=II,NML
        PX(I)=0.0
12      PY(I)=0.0
        II=NDB+1
        JJ=NDB+NBA
        ETA=0.0
        PHIF=ATAN(MUF)
        D1N=SIN(THETA+PHIF)
        D1D=COS(THETA+PHIF)
        D1=D1N/D1D
        DO 19 I=II,JJ
        A=ETA
        ETA=ETA+S(I)
        B=ETA
        SA=SIN(2.0*PI*A)
        SB=SIN(2.0*PI*B)
        CA=COS(2.0*PI*A)
        CB=COS(2.0*PI*B)
        SA1=SA/(2.0*PI)
        SB1=SB/(2.0*PI)
        SA2=SA/(8.0*(PI**3))
        SB2=SB/(8.0*(PI**3))
        SA3=SA/(32.0*(PI**5))
        SB3=SB/(32.0*(PI**5))
        CA1=CA/(4.0*(PI**2))
        CB1=CB/(4.0*(PI**2))
        CA2=CA/(16.0*(PI**4))
        CB2=CB/(16.0*(PI**4))
```

```
      CA3=CA/(64.0*(PI**6))
      CB3=CB/(64.0*(PI**6))
      IF (M.GT.0) GO TO 13
      D=D1
      PX(I)=(B-A-SB1+SA1)/D
      GO TO 18
13    IF (M.GT.1) GO TO 14
      D=0.5*D1
      PX(I)=((B**2)/2.0-(A**2)/2.0-B*SB1+A*SA1-CB1+CA1)/D
      GO TO 18
14    IF (M.GT.2) GO TO 15
      D=0.2826727*D1
      PX(I)=((B**3)/3.0-(A**3)/3.0-(B**2)*SB1+(A**2)*SA1
     1+2.0*SB2-2.0*SA2-2.0*B*CB1+2.0*A*CA1)/D
      GO TO 18
15    IF (M.GT.3) GO TO 16
      D=0.1740091*D1
      PX(I)=((B**4)/4.0-(A**4)/4.0-(B**3)*SB1+(A**3)*SA1
     1+6.0*B*SB2-6.0*A*SA2-3.0*(B**2)*CB1+3.0*(A**2)*CA1
     2+6.0*CB2-6.0*CA2)/D
      GO TO 18
16    IF (M.GT.4) GO TO 17
      D=0.1140778*D1 .
      PX(I)=((B**5)/5.0-(A**5)/5.0-(B**4)*SB1+(A**4)*SA1
     1+12.0*(B**2)*SB2-12.0*(A**2)*SA2-24.0*SB3+24.0*SA3
     2-4.0*(B**3)*CB1+4.0*(A**3)*CA1+24.0*B*CB2-24.0*A*CA2)/D
      GO TO 18
17    D=0.0785125*D1
      PX(I)=((B**6)/6.0-(A**6)/6.0-(B**5)*SB1+(A**5)*SA1
     1+20.0*(B**3)*SB2-20.0*(A**3)*SA2-120.0*B*SB3+120.0*A*SA3
     2-5.0*(B**4)*CB1+5.0*(A**4)*CA1+60.0*(B**2)*CB2
     3-60.0*(A**2)*CA2-120.0*CB3+120.0*CA3)/D
18    PY(I)=-D1*PX(I)
19    CONTINUE
      WRITE (6,301) (LOCT(I),PX(I),PY(I), I=1,NML)
C
C DETERMINATION OF PXS(I) AND PYS(I)
      DO 23 I=1,NML
      DO 22 J=1,NML
      RXB=XB(I)-XB(J)
      RYB=YB(I)-YB(J)
      IF (I.NE.J) GO TO 21
      B1(I,J)=0.0
      B2(I,J)=0.0
      B3(I,J)=0.0
      GO TO 22
21    PN=ANX(I)*RXB+ANY(I)*RYB
      PG=(RXB**2+RYB**2)**2
      B1(I,J)=-2.0*S(I)*PN*(RXB**2)/(PI*PG)
      B2(I,J)=-2.0*S(I)*PN*RXB*RYB/(PI*PG)
      B3(I,J)=-2.0*S(I)*PN*(RYB**2)/(PI*PG)
22    CONTINUE
23    CONTINUE
      DO 24 I=1,NML
      PXS(I)=PX(I)
      PYS(I)=PY(I)
24    CONTINUE
      NCICLE=1
      GO TO 27
25    IF (NCICLE.GT.40) GO TO 33
```

```
      NCICLE=NCICLE+1
      DO 26 I=1,NML
      PXS(I)=PXSN(I)
      PYS(I)=PYSN(I)
26    CONTINUE
27    DO 28 I=1,NML
      SUMX(I)=0.0
      SUMY(I)=0.0
28    CONTINUE
      DO 30 I=1,NML
      DO 29 J=1,NML
      SX=PXS(J)*B1(I,J)+PYS(J)*B2(I,J)
      SY=PXS(J)*B2(I,J)+PYS(J)*B3(I,J)
      SUMX(I)=SUMX(I)+SX
      SUMY(I)=SUMY(I)+SY
29    CONTINUE
30    CONTINUE
      DO 31 I=1,NML
      PXSN(I)=AL*PX(I)+(1.0-AL)*PXS(I)-AL*SUMX(I)
      PYSN(I)=AL*PY(I)+(1.0-AL)*PYS(I)-AL*SUMY(I)
31    CONTINUE
      DO 32 I=1,NML
      EPXS=PC*ABS(PXS(I))
      EPYS=PC*ABS(PYS(I))
      DPXS=ABS(PXSN(I)-PXS(I))
      DPYS=ABS(PYSN(I)-PYS(I))
      IF (DPXS.GT.EPXS) GO TO 25
      IF (DPYS.GT.EPYS) GO TO 25
32    CONTINUE
33    WRITE (6,401) NCICLE, (LOCT(I),PXSN(I),PYSN(I), I=1,NML)
C
C DETERMINATION OF SGMAXX(I),SGMAYY(I),SGMAXY(I)
      N=1
      L=1
      NEP=NEPI
34    DO 35 I=L,NEP
      SGMAXX(I)=0.0
      SGMAYY(I)=0.0
      SGMAXY(I)=0.0
35    CONTINUE
      DO 37 I=L,NEP
      DO 36 J=1,NML
      RXE=XE(I)-XB(J)
      RYE=YE(I)-YB(J)
      SN1=-2.0/(PI*((RXE**2+RYE**2)**2))
      SN2=PXSN(J)*RXE+PYSN(J)*RYE
      SNXX=SN1*SN2*(RXE**2)
      SNYY=SN1*SN2*(RYE**2)
      SNXY=SN1*SN2*RXE*RYE
      SGMAXX(I)=SGMAXX(I)+SNXX
      SGMAYY(I)=SGMAYY(I)+SNYY
      SGMAXY(I)=SGMAXY(I)+SNXY
36    CONTINUE
37    CONTINUE
      WRITE (6,100)
      WRITE (6,501) (LOCT(I),XE(I),YE(I), I=L,NEP)
      WRITE (6,601) (LOCT(I),SGMAXX(I),SGMAYY(I),SGMAXY(I), I=L,NEP)
C
C DETERMINATION OF SGMA1(I) AND SGMA2(I)
      DO 41 I=L,NEP
```

```
      IF (ABS(SGMAXX(I)-SGMAYY(I)).LT.0.00001) GO TO 38
      ALPHAA(I)=0.5*ATAN(2.0*SGMAXY(I)/(SGMAXX(I)-SGMAYY(I)))
      GO TO 39
38    ALPHAA(I)=PI/4.0
39    SGMAA(I)=SGMAXX(I)*(COS(ALPHAA(I))**2)+SGMAYY(I)*
     1 (SIN(ALPHAA(I))**2)+2.0*SGMAXY(I)*SIN(ALPHAA(I))*COS(ALPHAA(I))
      ALPHAB(I)=ALPHAA(I)+PI/2.0
      SGMAB(I)=SGMAXX(I)*(COS(ALPHAB(I))**2)+SGMAYY(I)*
     1 (SIN(ALPHAB(I))**2)+2.0*SGMAXY(I)*SIN(ALPHAB(I))*COS(ALPHAB(I))
      IF(SGMAA(I).GT.SGMAB(I)) GO TO 40
      SGMA1(I)=SGMAB(I)
      SGMA2(I)=SGMAA(I)
      ALPHA1(I)=ALPHAB(I)*(180.0/PI)
      ALPHA2(I)=ALPHAA(I)*(180.0/PI)
      GO TO 41
40    SGMA1(I)=SGMAA(I)
      SGMA2(I)=SGMAB(I)
      ALPHA1(I)=ALPHAA(I)*(180.0/PI)
      ALPHA2(I)=ALPHAB(I)*(180.0/PI)
41    CONTINUE
      WRITE (6,701) (LOCT(I),SGMA1(I),SGMA2(I),ALPHA1(I),
     1 ALPHA2(I), I=L,NEP)
C
C DETERMINATION OF K(I) AND PSI(I)
      IF (N.GT.1) GO TO 47
48    READ (5,DATA2)
      WRITE (6,DATA2)
47    J=1
      DO 42 I=L,NEP
      MU(I)=MUI
      C(I)=CI
      K(I,J)=(2.0*(C(I)-MU(I)*SGMAH))/(MU(I)*(SGMA1(I)+SGMA2(I))+
     1 (SQRT(1.0+MU(I)**2))*(SGMA1(I)-SGMA2(I)))
      PSI1(I)=ALPHA1(I)+45.0-((ATAN(MU(I)))/2.0)*(180.0/PI)
      PSI2(I)=ALPHA1(I)-45.0+((ATAN(MU(I)))/2.0)*(180.0/PI)
42    CONTINUE
      WRITE (6,800) J
      WRITE (6,802) (LOCT(I),K(I,J),PSI1(I),PSI2(I), I=L,NEP)
43    J=J+1
      JP=J-1
      DO 44 I=L,NEP
      SGMAM(I)=(K(I,JP)*(SGMA1(I)+SGMA2(I))/2.0)+SGMAH
      IF (SGMAM(I).LT.SIGMAX) GO TO 61
    TAU(I)=T0+T1*(SGMAM(I))+T2*(SGMAM(I)**2)+T3*(SGMAM(I)**3)+
     1 T4*(SGMAM(I)**4)+T5*(SGMAM(I)**5)+T6*(SGMAM(I)**6)+
     2 T7*(SGMAM(I)**7)
    SIG(I)=S0+S1*(SGMAM(I))+S2*(SGMAM(I)**2)+S3*(SGMAM(I)**3)+
     1 S4*(SGMAM(I)**4)+S5*(SGMAM(I)**5)+S6*(SGMAM(I)**6)+
     2 S7*(SGMAM(I)**7)
      MU(I)=(SIG(I)-SGMAM(I))/TAU(I)
      C(I)=TAU(I)+SIG(I)*MU(I)
      GO TO 62
61    MU(I)=0.0
      C(I)=TAUMAX
62    K(I,J)=(2.0*(C(I)-MU(I)*SGMAH))/(MU(I)*(SGMA1(I)+SGMA2(I))+
     1 (SQRT(1.0+MU(I)**2))*(SGMA1(I)-SGMA2(I)))
      PSI1(I)=ALPHA1(I)+45.0-((ATAN(MU(I)))/2.0)*(180.0/PI)
      PSI2(I)=ALPHA1(I)-45.0+((ATAN(MU(I)))/2.0)*(180.0/PI)
44    CONTINUE
      WRITE (6,800) J
```

```
      WRITE (6,801) (LOCT(I),SGMAM(I),MU(I),C(I),  I=L,NEP)
      WRITE (6,802) (LOCT(I),K(I,J),PSI1(I),PSI2(I), I=L,NEP)
      IF (J.GT.9) GO TO 46
      DO 45 I=L,NEP
      EK=0.010*ABS(K(I,JP))
      DK=ABS(K(I,J)-K(I,JP))
      IF (DK.GT.EK) GO TO 43
45    CONTINUE
46    CONTINUE
      KMIN=K(L,J)
      X=XF(L)
      Y=YF(L)
      II=L+1
      DO 49 I=II,NEP
      IF (K(I,J).LT.0.0) GO TO 49
      IF (K(I,J).GE.KMIN) GO TO 49
      KMIN=K(I,J)
      X=XF(I)
      Y=YF(I)
49    CONTINUE
      WRITE (6,901) J,KMIN
C
C FURTHER SUBDIVISION OF FIELD
      N=N+1
      IF (NEP.EQ.NEPI) GO TO 50
      N=1
      L=1
      NEP=NEPI
      GO TO 48
50    L=NEP+1
      NEP=NEP+22
      II=L+7
      JJ=NEP-4
      DO 51 I=II,JJ,5
51    XF(I)=X-2.0*DIV
      II=L+3
      JJ=NEP-3
      DO 52 I=II,JJ,5
52    XF(I)=X-DIV
      XF(L)=X
      II=L+4
      JJ=NEP-2
      DO 53 I=II,JJ,5
53    XF(I)=X
      XF(L+1)=X+DIV
      II=L+5
      JJ=NEP-1
      DO 54 I=II,JJ,5
54    XF(I)=X+DIV
      XF(L+2)=X+2.0*DIV
      II=L+6
      DO 55 I=II,NEP,5
55    XF(I)=X+2.0*DIV
      JJ=L+2
      DO 56 I=L,JJ
56    YF(I)=Y+2.0*DIV
      II=L+3
      JJ=L+6
      DO 57 I=II,JJ
57    YF(I)=Y+DIV
```

```
      II=L+7
      JJ=L+11
      DO 58 I=II,JJ
 58   YF(I)=Y
      II=L+12
      JJ=L+16
      DO 59 I=II,JJ
 59   YF(I)=Y-DIV
      II=L+17
      DO 60 I=II,NEP
 60   YF(I)=Y-2.0*DIV
      GO TO 34
      END
$ENDFILE
$RUN -LOAD+*SSP UAP 5=*SOURCE* 6=*SINK*
$SIGNOFF
$ENDFILE
                                                    377 LINES
```

Table 1

Fracture Initiation Results for Blair dolomite and quartzite; $m = 5$, $\mu_f = 0.0$

Material	θ	$\bar{\sigma}^H$(kb)	K_{min}	$\bar{\sigma}_m$(kb)
Blair dolomite	45^o	-3.0	4.185	-11.3
		-2.0	4.185	-10.3
		-1.0	4.185	- 9.3
		-0.5	3.946	- 4.9
		0.0	2.708	- 2.65
	30^o	-2.0	3.035	-10.4
	60^o	-2.0	4.774	- 9.5
quartzite	45^o	-0.5	5.278	- 5.25
		0.0	2.953	- 2.48

Table A-1

Points obtained From Mohr Envelope of Blair Dolomite

$\bar{\sigma}_m$ (kb)	$\bar{\tau}$ (kb)	$\bar{\sigma}$ (kb)
-.7	.25	.4
-.9	.5	.3
-1.4	1.0	0.0
-2.0	1.3	-.25
-2.5	1.6	-.45
-3.6	2.4	-1.2
-4.4	3.1	-1.95
-5.9	4.2	-3.5
-6.45	4.75	-4.65
-7.1	5.1	-5.7
-8.2	5.5	-7.4
-9.1	5.6	-9.0
-10.0	5.6	-10.0
-11.0	5.6	-11.0

Table A-2

Points obtained From Mohr Envelope of Quartzite

$\bar{\sigma}_m$ (kb)	$\bar{\tau}$ (kb)	$\bar{\sigma}$ (kb)
-.2	.2	.3
-1.2	.6	.1
-3.4	1.5	-.4
-4.7	2.2	-.8
-6.2	3.3	-1.5
-9.0	4.6	-2.4
-11.0	6.0	-3.6
-11.65	7.2	-4.6
-12.65	8.1	-5.55
-14.0	8.75	-6.4
-14.8	9.55	-7.35
-15.8	10.4	-8.5
-16.95	11.4	-10.1
-17.5	12.3	-12.0

Table A-3

Coefficients of Least-squares Polynomial Fits

	Blair dolomite	quartzite
α_0	.90932523	.14589997
α_1	-2.2527893	-.39293411
α_2	- .98623052	-.11661122
α_3	- .27366620	-.07536858
α_4	- .03557571	-.01643163
α_5	- .00211718	-.00168279
α_6	- .00004702	-.00008117
α_7	.00000000	-.00000149
S	.058635	.257773
β_0	.64800776	.37275022
β_1	.25671860	.44518983
β_2	-.22792865	.32929945
β_3	-.10632980	.14898031
β_4	-.02453351	.02914393
β_5	-.00222438	.00282896
β_6	-.00006876	.00013247
β_7	.00000000	.00000239
S	.113464	.205440

ACKNOWLEDGMENTS

The authors gratefully acknowledge the financial support of the National Science Foundation under Grant No. GK 37289.

REFERENCES

1. Sikarskie, D. L. and Altiero, N. J., "The Formation of Chips in the Penetration of Elastic-Brittle Materials (Rock)," Journal of Applied Mechanics, Vol. 40, No. 3, Trans. ASME, Vol. 95, Series E, Sept. 1973, pp 791-798.

2. Benjumea, R. and Sikarskie, D. L., "On the Solution of Plane, Orthotropic Elasticity Problems by an Integral Method, "Journal of Applied Mechanics, Vol. 39, Trans ASME, Vol. 94, Series E, Sept. 1972, pp. 801-808.

3. Paul, B., "Macroscopic Criteria for Flow and Fracture, "Fracture: An Advanced Treatise, Vol. II, ed., Liebowitz, H., Academic Press, New York and London, 1968, Chapter 4.

4. Bieniawski, Z. T., "Mechanism of Brittle Fracture of Rock," International Journal of Rock Mech. Min. Sci., Vol. 4, 1967, pp. 395-430.

5. Brace, W. F., "Brittle Fracture of Rocks, "State of Stress in the Earth's Crust, ed., Judd, W., Elsevier, New York, 1964.

6. Brace, W. F., Silver, E., Hadley, K. and Goetze, C., Cracks and Pores: A Closer Look, "Science, Vol. 178, 13 October 1972, pp. 162-164.

7. Carnahan, B., Luther, H. A. and Wilkes J. O., Applied Numerical Methods, John Wiley and Sons, Inc., New York, 1969, pp. 574-584.

8. Robertson, E. C., "Experimental Study of the Strength of Rocks," Bulletin of the Geological Society of America, Vol. 66, October, 1955, pp. 1275-1314.

9. Gnirk, P. F. and Cheatham, J. B., "An Experimental Study of Single Bit-Tooth Penetration into Dry Rock at Confining Pressures of 0 to 5000 psi, "Society of Petroleum Engineers Journal, AIME Trans., Vol. 234, 1965, pp. 117-130.

FIGURE CAPTIONS

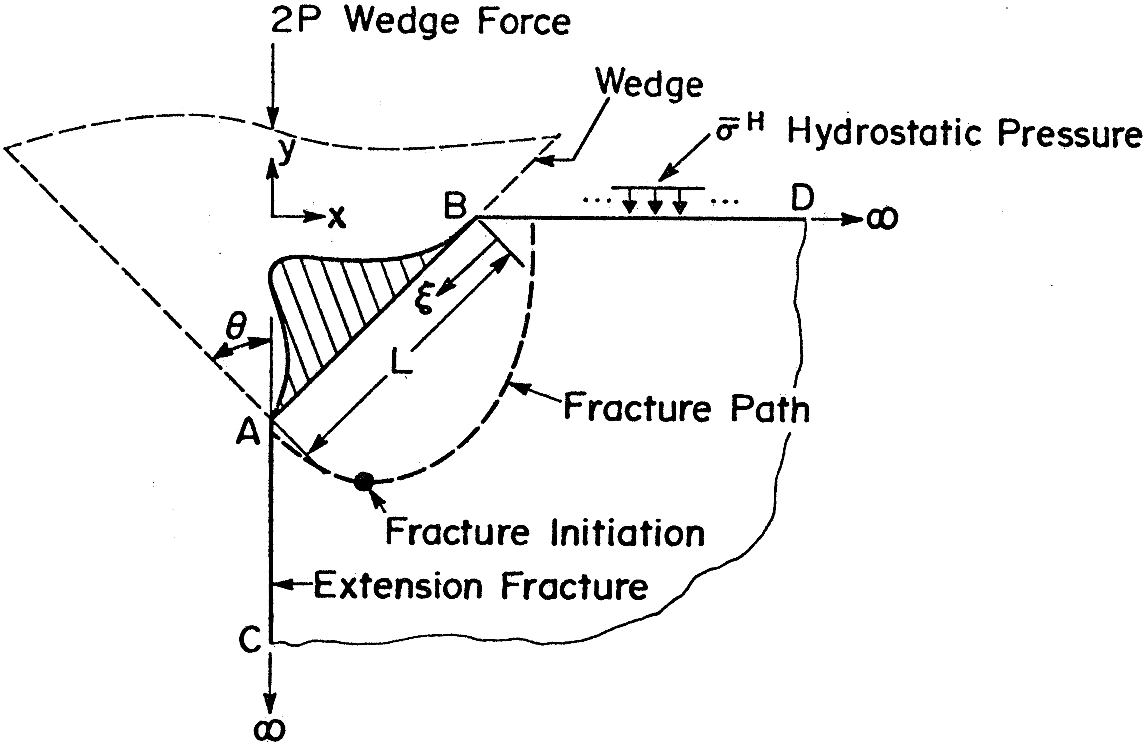
2P Wedge Force
Wedge
$\bar{\sigma}^H$ Hydrostatic Pressure
y
x
B
D
∞
ξ
θ
L
A
Fracture Path
Fracture Initiation
Extension Fracture
C
∞

Figure 1

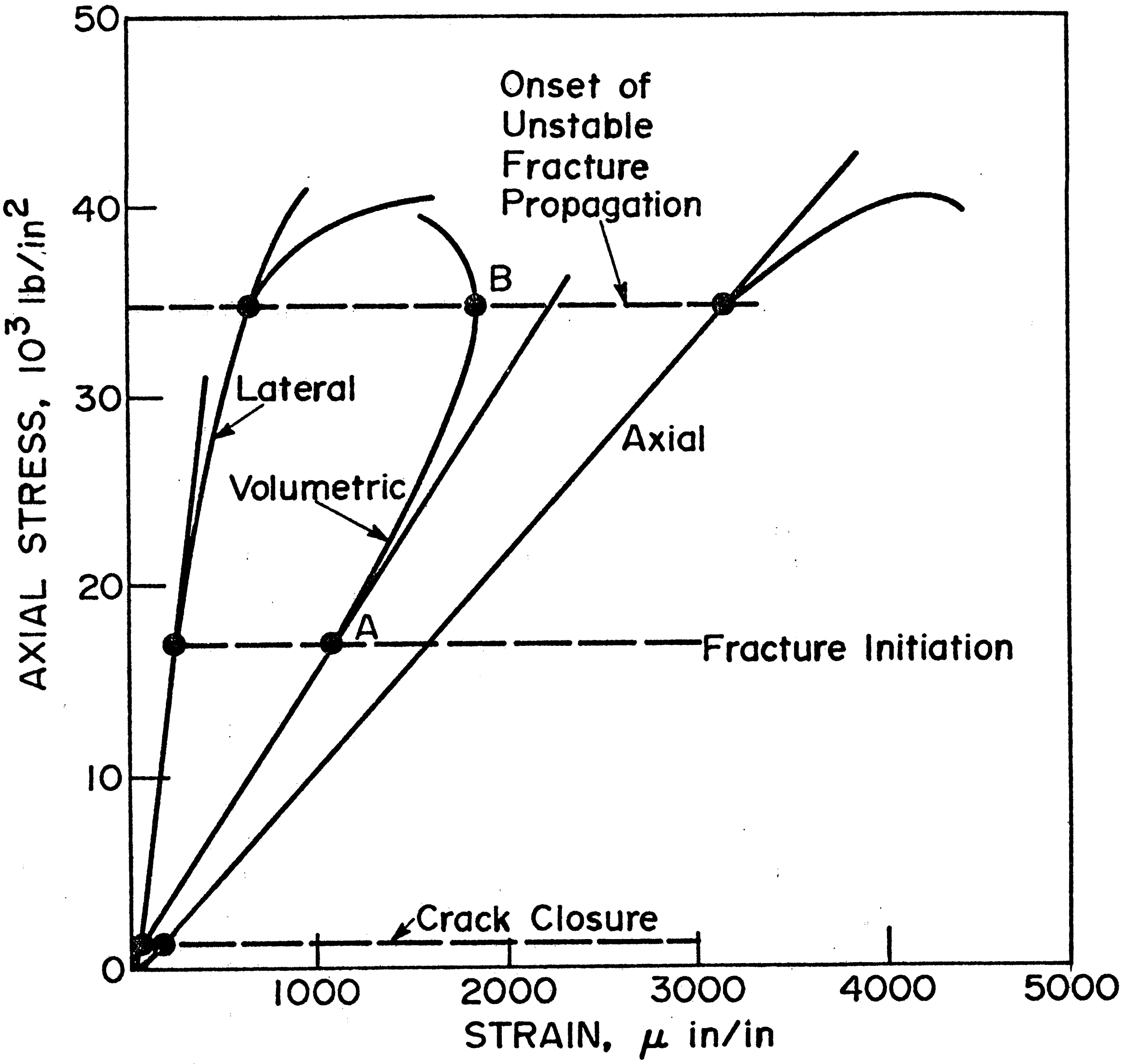

Onset of
Unstable
Fracture
Propagation
B
Lateral
Volumetric
Axial
A
Fracture Initiation
Crack Closure
AXIAL STRESS, 10^3 lb/in^2
STRAIN, μ in/in
50
40
30
20
10
0
1000
2000
3000
4000
5000

Figure 2

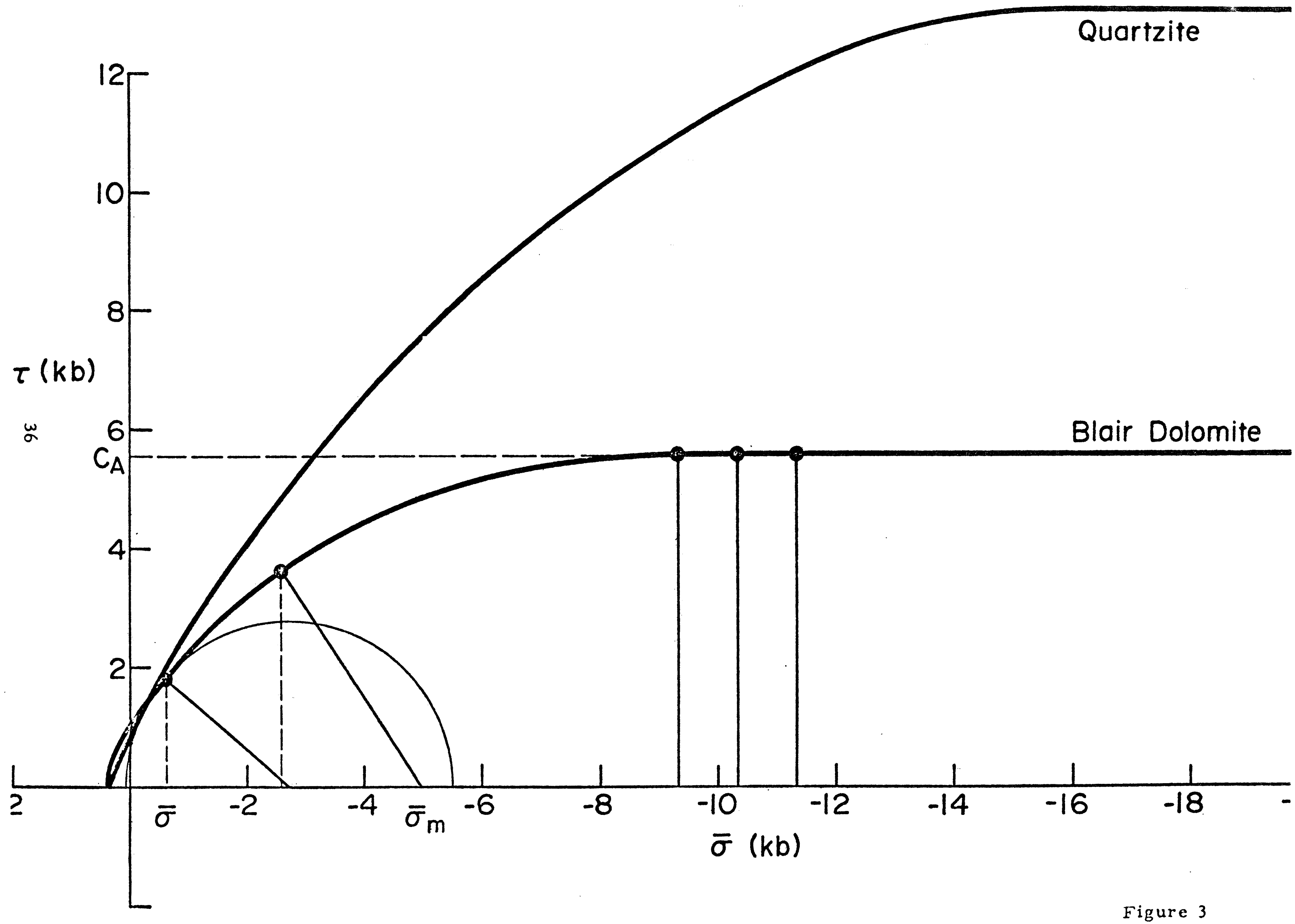

Quartzite
Blair Dolomite
τ (kb)
12
10
8
6
C_A
4
2
2
$\bar{\sigma}$
-2
-4
$\bar{\sigma}_m$
-6
-8
-10
-12
-14
-16
-18
$\bar{\sigma}$ (kb)

Figure 3

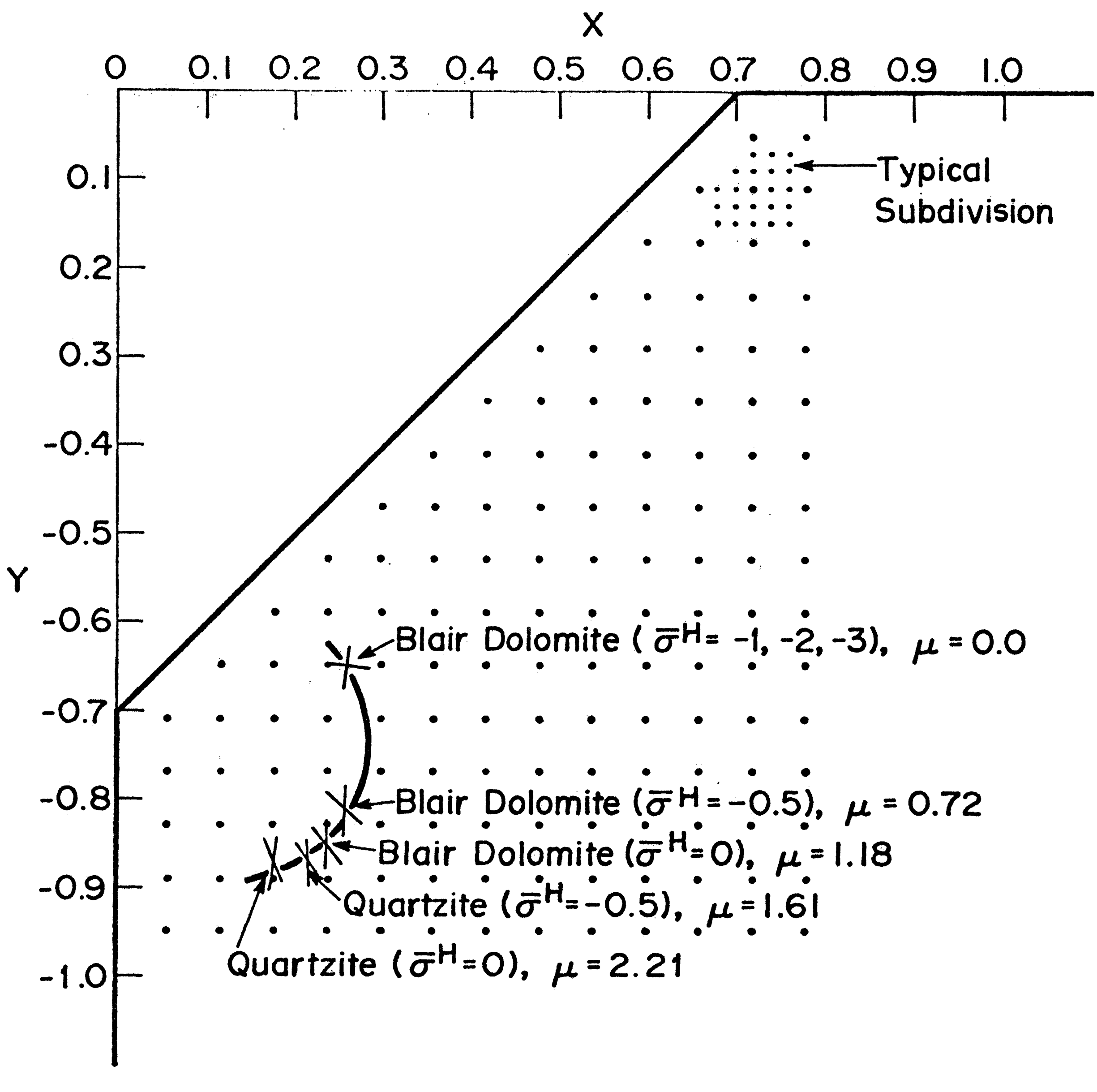

X
0
0.1
0.2
0.3
0.4
0.5
0.6
0.7
0.8
0.9
1.0
Y
0.1
0.2
0.3
-0.4
-0.5
-0.6
-0.7
-0.8
-0.9
-1.0
Typical Subdivision
Blair Dolomite ($\bar{\sigma}^H$= -1, -2, -3), μ = 0.0
Blair Dolomite ($\bar{\sigma}^H$ = -0.5), μ = 0.72
Blair Dolomite ($\bar{\sigma}^H$=0), μ = 1.18
Quartzite ($\bar{\sigma}^H$=-0.5), μ = 1.61
Quartzite ($\bar{\sigma}^H$=0), μ = 2.21

Figure 4

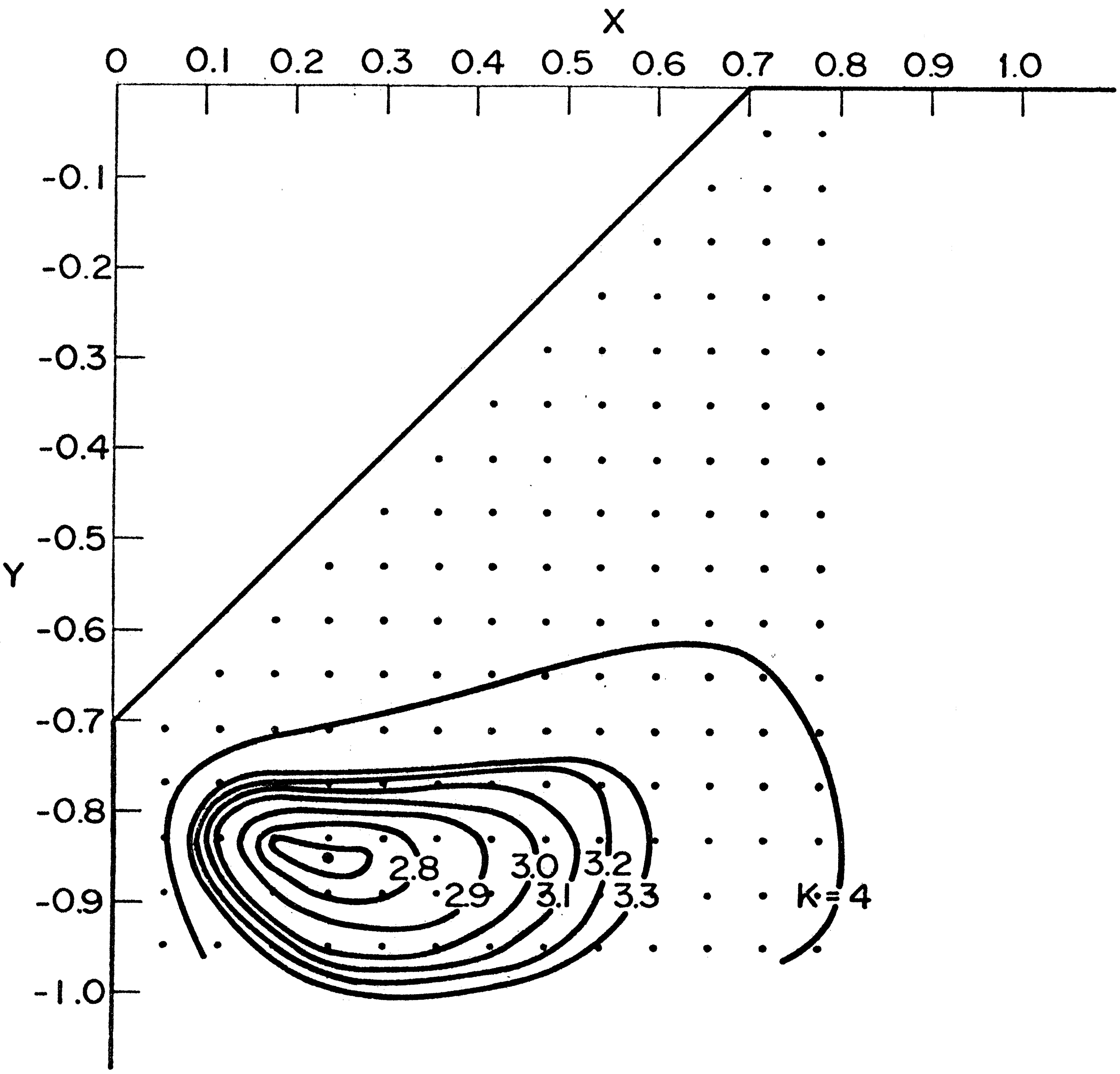
X
0
0.1
0.2
0.3
0.4
0.5
0.6
0.7
0.8
0.9
1.0
Y
-0.1
-0.2
-0.3
-0.4
-0.5
-0.6
-0.7
-0.8
-0.9
-1.0
2.8
2.9
3.0
3.1
3.2
3.3
K = 4

Figure 5

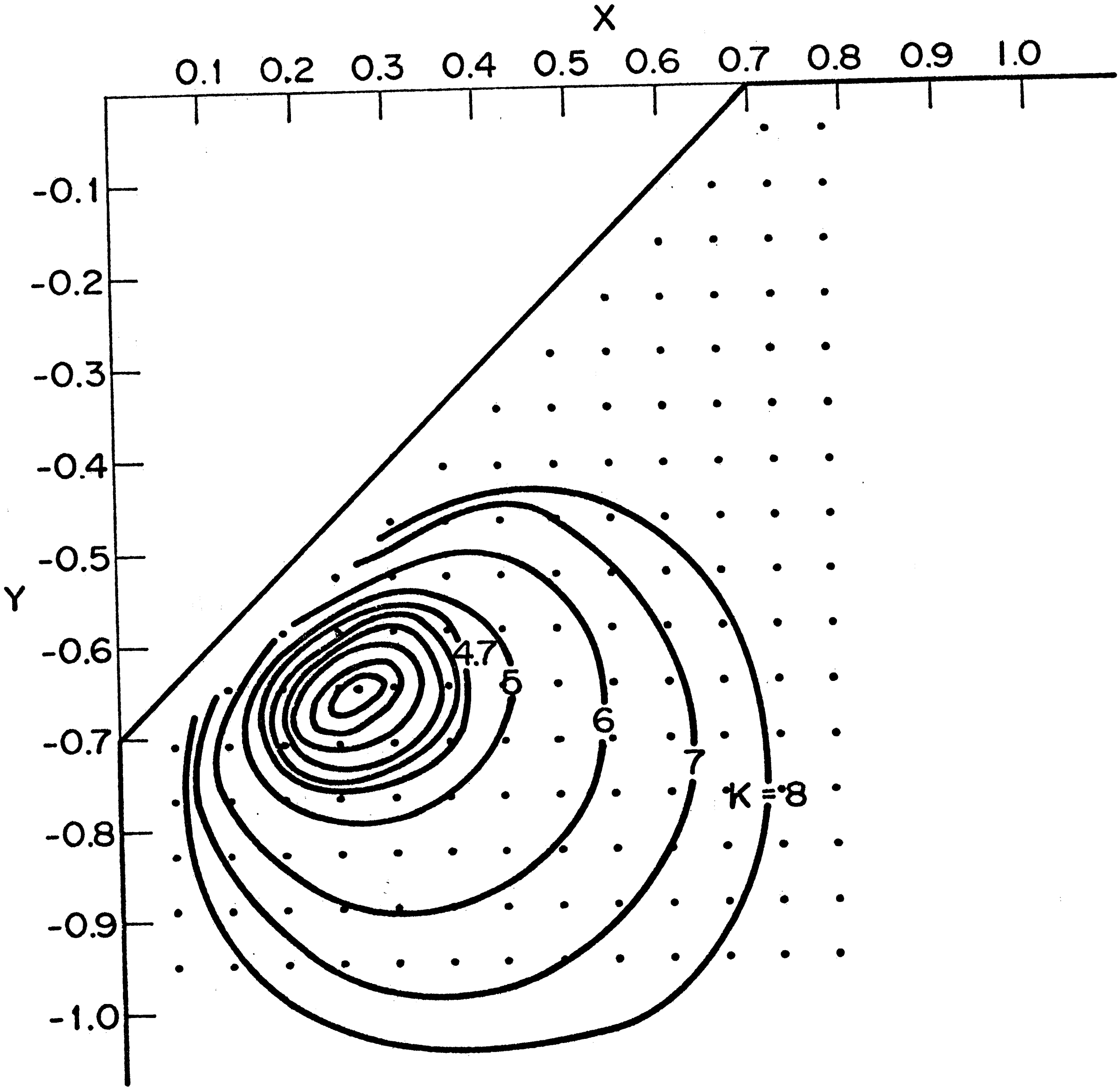

Figure 6

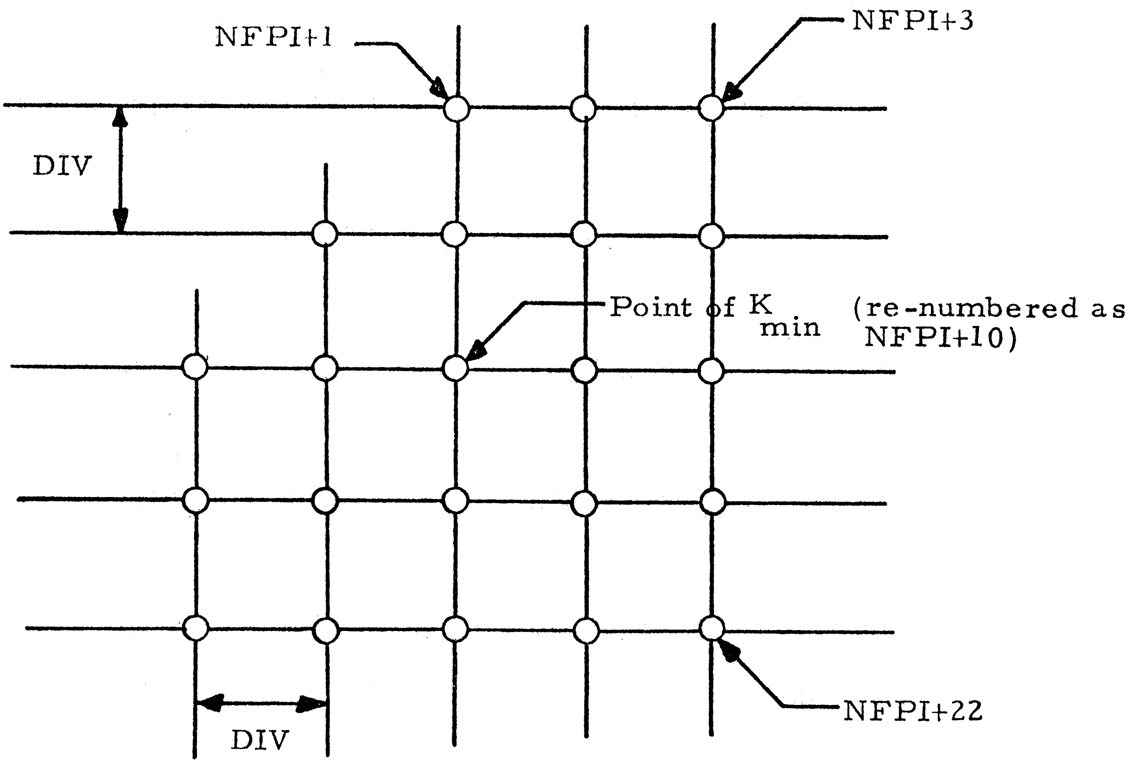
NFPI+1
NFPI+3
DIV
Point of K_{min} (re-numbered as NFPI+10)
NFPI+22
DIV

Figure B-1